Sciencexpress Report

# High-Latitude Forcing of the South American Summer Monsoon During the Last Glacial

Lisa C. Kanner,[1]* Stephen J. Burns,[1] Hai Cheng,[2,3] R. Lawrence Edwards[3]

[1]Department of Geosciences, University of Massachusetts, Amherst, MA 01002, USA. [2]Institute of Global Environmental Change, Xi'an Jiaotong University, Xi'an 710049, China. [3]Department of Geology and Geophysics, University of Minnesota, Minneapolis, MN 55455, USA.

*To whom correspondence should be addressed. E-mail: lkanner@geo.umass.edu

**The climate of the Last Glacial period (10,000-110,000 years ago) was characterized by rapid millennial-scale climate fluctuations termed Dansgaard/Oeschger (D/O) and Heinrich (H) events. We present results from a speleothem-derived proxy of the South American Summer Monsoon (SASM) from 16,000-50,000 years ago that demonstrate the occurrence of D/O cycles and Heinrich events. This tropical Southern Hemisphere monsoon reconstruction illustrates an anti-phase relationship to Northern Hemisphere monsoon intensity at the millennial scale. Our results also show an influence of Antarctic millennial-scale climate fluctuations on the SASM. This high-resolution, precisely dated, tropical precipitation record can be used to establish the timing of climate events in the high latitudes of the Northern and Southern Hemispheres.**

D/O and Heinrich events have been recognized in many terrestrial and marine records, particularly from the Northern Hemisphere. First observed in oxygen isotope ratios of ice cores from Greenland (*1*), the D/O cycles are interpreted as large abrupt warmings (interstadials) followed by more gradual cooling to stadial conditions. The D/O cycles are particularly well expressed in tropical Northern Hemisphere speleothem records, where cold and warm periods in Greenland are coincident with dry and wet periods, respectively, in the East Asian and Indian Summer Monsoons (EASM and ISM) (*2*–*4*). The presence of D/O cycles in the Southern Hemisphere, or their relationship to Southern Hemisphere monsoons, has not been established, however. Heinrich events are pronounced cold intervals (~500 ± 250 years in duration) marked by horizons of ice rafted debris in ocean sediment cores from mid-latitudes in the Atlantic Ocean (*5*–*7*). While an interhemispheric anti-phased relationship has been observed for the Heinrich (H1-H6) events, the specific timing and duration is less well constrained due to uncertainties in ocean reservoir ages (*8*) and changes in sediment accumulation rates. Here, we present a high resolution, precisely-dated, speleothem reconstruction of SASM intensity for the Last Glacial period that demonstrates the presences of D/O cycles in the SASM, where an intensified SASM is associated with stadial events in Greenland. In addition, we identify millennial-scale climate events that result from the interplay between rapid Antarctic warming and cool North Atlantic Heinrich events. Finally, we use the signature of the major of D/O cycles to propose possible constraints on the timing and duration of Heinrich events H4 and H5.

We collected stalagmite P09-PH2 from Pacupahuain Cave (11.24°S, 75.82°W; 3800 meters above sea level) in the central Peruvian Andes (fig. S1). Pacupahuain Cave was formed in a Triassic dolomitic limestone massif (*9*) and from an area where glacial landforms are not present. P09-PH2 is a calcite stalagmite 16 centimeters tall, which was collected in the cave's main gallery about 500 meters from the entrance. The speleothem was halved along the growth axis and subsampled along growth layers for radiometric dating using uranium-thorium (U-Th) techniques by multi-collector, inductively coupled plasma mass spectroscopy (MC-ICP-MS) (*10*, *11*). Seventeen $^{230}$Th dates, all in stratigraphic order, have analytical errors < 0.4% (fig. S2, table S1). An age model was developed based on linear interpolation between adjacent age measurements, yielding an age range for the sample of 16,020 to 49,470 years before present [(BP), present = 1950].

Stable oxygen and carbon isotope ratios ($\delta^{18}$O and $\delta^{13}$C) were measured on 1076 micromilled samples taken along the growth axis. Average sampling resolution is approximately 30 years. The very low correlation ($r^2 = 0.1$) between $\delta^{13}$C and $\delta^{18}$O values along the growth axis (fig. S3) indicates that kinetic fractionation does not significantly influence speleothem isotopic variability (*11*, *12*). P09-PH2 $\delta^{18}$O values range from –14‰ to –17.5‰ between 16 and 50 kyr BP (Fig. 1). The $\delta^{18}$O record is characterized by high amplitude millennial-scale events with rapid increases of up to 2.5‰ occurring over a century or less. The decline to local $\delta^{18}$O minima occurs more gradually, over a few centuries to a few millennia. The lowest values in the record occur over an extended period of time between 28.8-30.3 kyr BP. The highest values are attained over very brief intervals at 16, 37, 38, and 47 kyr BP.

We interpret the changes in speleothem calcite to be primarily driven by changes in the isotopic composition of precipitation at the site. Two additional factors, changes in cave temperature and changes in the isotopic composition of seawater, also contribute to the observed variability, but serve primarily to reduce the amplitude of isotopic change by a maximum of about 1.5 ‰ (*11*). Thus, P09-PH2 records the minimum amplitude of changes in $\delta^{18}O$ of precipitation and actual changes were likely larger. What, then, drives changes in $\delta^{18}O$ of precipitation at the study site?

The primary climatic control on rainfall $\delta^{18}O$ for tropical South America is precipitation amount (*13*). Consistent with the 'amount effect' (*14*) and Rayleigh-type fractionation during rainout, a stronger SASM leads to lower $\delta^{18}O$ values in tropical South American rainfall (*15*). Similar correlations have been made for other parts of the tropical Andes, where local precipitation $\delta^{18}O$ is strongly anticorrelated to rainfall amount upstream in the Amazon Basin rather than at the study site (*16*, *17*). Rayleigh distillation and moisture recycling in the Amazon Basin (*18*) preserve isotopic signal of the monsoon along the moisture path from eastern Amazonia up to the central Peruvian Andes (*15*). On interannual timescales, the SASM is influenced by sea surface temperatures in the Atlantic and Pacific Oceans (*19*) and on orbital timescales by changes in insolation (*20*, *21*). These studies demonstrate that rainfall $\delta^{18}O$ in the central Andes records changes in the intensity of large-scale continental atmospheric convection, with more negative rainfall $\delta^{18}O$ values indicative of enhanced SASM activity and increased rainout.

Comparing the millennial-scale variability in the Pacupahuain Cave record to the isotopic fluctuations from Greenland (Fig. 1) shows that all D/O cycles are also found in our record of SASM intensity, with the sole exception of D/O event 3, which for unknown reasons, is not present. Identification of D/O events is based on comparison to the North Greenland Ice core Project (NGRIP) oxygen isotope record using the ice core age model of (*22*) (Fig. 1) and the MSD speleothem record from Hulu Cave, China using its own precise chronology (fig. S4) (*4*, *11*). Abrupt increases in NGRIP $\delta^{18}O_{ice}$, which characterize the onset of the D/O events, are clearly associated with rapid increases in $\delta^{18}O_{calcite}$ for P09-PH2. The relationship between D/O events in the NGRIP record and our results demonstrates that warm events in Greenland correspond to intervals of decreased SASM intensity. The timing of millennial-scale variability is synchronous within the independent age model errors.

Figure 1 also includes the record of atmospheric methane concentrations from Greenland and Antarctic ice cores (*23*–*25*). The origin of millennial-scale variations in atmospheric methane is not certain, though they are thought to arise from changes in the flux from global wetlands (*26*, *27*) rather than release of $CH_4$ from marine clathrates (*28*) or changes in $CH_4$ removal via oxidation in the troposphere (*26*). Yet, whether source flux changes derive from tropical wetlands or boreal forests has not been established. We observe that increases in global atmospheric methane occur contemporaneously with increases in P09-PH2 $\delta^{18}O$ and reduced in SASM intensity (Fig. 1). Thus, the Southern Hemisphere South American tropics are unlikely to be a source of increased atmospheric methane, via wetland expansion, during Greenland interstadials. The interhemispheric antiphasing of the tropical monsoon systems during D/O events, however, indicates that rapid northward shifts of the ITCZ and intensification of the EASM and ISM might lead to wetland expansion and increased methane production in the Northern Hemisphere tropics during warm Greenland intervals.

In addition to the millennial-scale D/O events, each Heinrich event (H1 through H5) can also be identified in the P09-PH2 reconstruction by periods of enhanced SASM activity (Fig. 1) and by correlation to decreased Asian monsoon intensity based on the Hulu Cave record (fig. S4) (*4*, *11*). Previous paleoclimate studies of the SASM, which reconstructed precipitation intensity during the last glacial period but at lower resolution than presented here, also identified Heinrich events as particularly wet intervals (*29*, *30*). Increased Heinrich event precipitation over tropical South America is supported by evidence of significant lateral advancement of central Andean glaciers during H1 and H2 (*31*) and increases in precipitation over northeast Brazil for H1 through H5 (*30*, *32*, *33*).

The expression of D/O cycles and Heinrich events in SASM variability is anti-phased with Northern Hemisphere monsoon precipitation reconstructions over the Last Glacial period. Our record indicates a weak SASM during D/O interstadials, but reconstructions of Indian Ocean climate (*2*) and EASM intensity (*4*) demonstrate very wet intervals for interstadial phases. While previous work has demonstrated such antiphase behavior for orbital scale climate variability in the tropics (*21*) and for Heinrich events (*30*), it had not been unequivocally determined for D/O scale variability. Such anti-phase behavior can be explained by latitudinal shifts of the Inter-Tropical Convergence Zone (ITCZ) driven by rapid Northern Hemisphere temperature fluctuations. Modeling data demonstrate ITCZ migration away from the hemisphere with high latitude cooling and added ice cover (*34*). During pronounced North Atlantic cold events, southward migration of the ITCZ can alter Hadley cell circulation, increase subsidence (dry conditions) for the northern branch and intensify uplift (wet conditions) of the southern branch (*35*, *36*). As a result, the ISM and EASM weaken and the SASM intensifies. Although our record is short relative to precessional scale insolation changes, insolation appears to be only weakly expressed in our record (fig. S5).

In addition to demonstrating the presence of D/O and Heinrich variability in the SASM, our record reveals additional rapid, millennial scale climate reversals in the tropical climate record. These events appear to arise from the interplay between Northern and Southern high latitude climate change. The reversals are most clearly expressed at 38.75 and 48 kyr BP during extended Greenland stadials (Fig. 2). We propose that the onset of these events coincide with the onset of Antarctic Isotope Maxima (AIM) events 8 and 12 in the EPICA Dronning Maud Land (EDML) ice core record (*22*). Prolonged Greenland cold phases have been linked with intensification and southward displacement of the Southern Hemisphere westerlies, enhanced upwelling in the Southern Ocean, rising atmospheric $CO_2$, and Antarctic warming (*37*, *38*). Specifically, the opal flux reconstruction presented in (*38*) demonstrates that ocean upwelling and $CO_2$ rises were largest during H4 and H5 compared to younger Heinrich events. Thus, we propose that enhanced changes in Southern Ocean climate specific to H4 and H5 can explain why our record shows reversals in SASM vigor at H4 and H5 and not for the later Heinrich events.

The precise relationship between these transient millennial-scale events and ice-rafted components of Heinrich events H4 and H5, which occur at approximately the same time period, is less clear. It is well established that the endings of H4 and H5 occur with Greenland warming at D/O events 8 and 12, respectively, but the beginning of H4 and H5 is less well constrained. One interpretation based on our record is that the onset of Heinrich events H4 and H5 began with the sharp increase in SASM intensity that follows the decrease associated with Antarctic warming. An abrupt increase in SASM intensity associated with Heinrich events has been recognized in marine (*32*, *33*) and terrestrial records (*29*, *30*). This sequence of events would restrict the duration of H4 and H5 events to <400, which has previously been suggested for H4 (*39*). It would also indicate that Antarctic warming precedes the start of Heinrich events 4 and 5. We note that Antarctic warming has previously been proposed as a trigger for H1 (*40*). A second possibility, however, is that H4 and H5 may have begun prior to weakening of the SASM and Antarctic warming and thus lasted throughout the extended Greenland cold phase. Although in this case, we have no explanation for why the SASM suddenly strengthened.

One final aspect of the SASM reversals prior to D/O events 8 and 12 is unusual. High northern latitude warming is associated with an intensification of the NH monsoons. By analogy, high southern latitude warming might be expected to result in intensification of the SASM, but the opposite is observed. This seeming contradiction can be reconciled by comparison of our record to a high resolution sea surface temperature (SST) record based on alkenone paleothermometry from the Bermuda Rise (33.69°N, 57.56°W) (*41*). Core MD95-2036 shows large rapid warm intervals (3° to 5°C) immediately prior to D/O events 8 and 12, which were originally interpreted as instabilities during the rapid transitions of the largest Greenland interstadials. Based on visual comparison, we establish tie points between the Bermuda Rise SST record and our $\delta^{18}O$ record and provide a revised age model for these two oscillations in Bermuda Rise SSTs (*11*) (Fig. 3). The original marine core chronology was based on maximizing the correlation to the Greenland ice core record and its chronology at the time of publication (*11*, *42*). Our revised chronology for the two intervals of MD95-2036 places the warm intervals 600 ± 100 years earlier, relative to an updated Greenland chronology, which is well within the thousand-year uncertainty of the original marine core age model. Thus, Antarctic warming at AIM events 8 and 12 may be associated with a weakened SASM as described above (Fig. 2), as well as a warmer subtropical North Atlantic Ocean (Fig. 3) (*41*). It is interesting to note that similar temperature reversals within H4 and H5 have been identified in a deep water record from the Iberian Margin (*43*). While it is not clear why Antarctic warming is associated with warming in the subtropical North Atlantic, although one result of the latter could be a northward shift of the ITCZ in the Atlantic Ocean sector (*44*) due to a weakening of the subtropical Atlantic gyre. The association between warm SSTs in the Bermuda Rise region, a weakening of the SASM, and a more northerly position of the ITCZ, as we have described for the D/O events, could also be applied to the additional reversals identified in Fig. 3.

## References and Notes


1. W. Dansgaard *et al.*, Evidence for General Instability of Past Climate from a 250-Kyr Ice-Core Record. *Nature* **364**, 218-220 (1993).
2. S. J. Burns, D. Fleitmann, A. Matter, J. Kramers, A. A. Al-Subbary, Indian Ocean climate and an absolute chronology over Dansgaard/Oeschger events 9 to 13. *Science* **301**, 1365-1367 (2003).
3. Y. Wang *et al.*, Millennial- and orbital-scale changes in the East Asian monsoon over the past 224,000 years. *Nature* **451**, 1090-1093 (2008). doi: 10.1038/nature06692
4. Y. J. Wang *et al.*, A High-Resolution Absolute-Dated Late Pleistocene Monsoon Record from Hulu Cave, China. *Science* **294**, 2345-2348 (2001). doi: 10.1126/science.1064618
5. H. Heinrich, Origin and Consequences of Cyclic Ice Rafting in the Northeast Atlantic-Ocean during the Past 130,000 Years. *Quat. Res.* **29**, 142-152 (1988).

6. G. Bond *et al.*, Evidence for Massive Discharges of Icebergs into the North-Atlantic Ocean during the Last Glacial Period. *Nature* **360**, 245-249 (1992).
7. S. R. Hemming, Heinrich events: Massive late Pleistocene detritus layers of the North Atlantic and their global climate imprint. *Rev. Geophys.* **42**, RG000128 (2004). doi: 10.1029/2003rg000128
8. T. F. Stocker, The effect of a succession of ocean ventilation changes on C-14. *Radiocarbon* **40**, 359-366 (1998).
9. E. J. Cobbing *et al.*, in *The Geology of the Western Cordillera of Northern Peru* (Great Britian Institute of Geological Sciences, Natural Environmental Research Council, 1981), pp. 143.
10. H. Cheng *et al.*, Timing and structure of the 8.2 kyr B.P. event inferred from $^{18}$O records of stalagmites from China, Oman, and Brazil. *Geology* **37**, 1007-1010 (2009). doi: 10.1130/g30126a.1
11. Information on materials and methods is available on *Science* Online.
12. C. H. Hendy, Isotopic Geochemistry of Speleothems .1. Calculation of Effects of Different Modes of Formation on Isotopic Composition of Speleothems and Their Applicability as Palaeoclimatic Indicators. *Geochim. Cosmochim. Acta* **35**, 801-824 (1971).
13. M. Vuille, R. S. Bradley, M. Werner, R. Healy, F. Keimig, Modeling $\delta^{18}$O in precipitation over the tropical Americas: 1. Interannual variability and climatic controls. *J. Geophys. Res.* **108**, (2003). doi: 10.1029/2001jd002038
14. W. Dansgaard, Stable Isotopes in Precipitation. *Tellus* **16**, 436-468 (1964).
15. M. Vuille, M. Werner, Stable isotopes in precipitation recording South American summer monsoon and ENSO variability: observations and model results. *Clim. Dyn.* **25**, 401-413 (2005). doi: 10.1007/S00382-005-0049-9
16. F. Vimeux, R. Gallaire, S. Bony, G. Hoffmann, J. Chiang, What are the climate controls on $\delta$D in precipitation in the Zongo Valley (Bolivia)? Implications for the Illimani ice core interpretation. *Earth Planet. Sci. Lett.* **240**, 205-220 (2005). doi: 10.1016/j.epsl.2005.09.031
17. G. Hoffmann *et al.*, Coherent isotope history of Andean ice cores over the last century. *Geophys. Res. Lett.* **30**, 1178 (2003). doi: 10.1029/2002gl014870
18. R. L. Victoria, L. A. Martinelli, J. Mortatti, J. Richey, Mechanisms of Water Recycling in the Amazon Basin - Isotopic Insights. *Ambio* **20**, 384-387 (1991).
19. M. Vuille, R. S. Bradley, F. Keimig, Interannual climate variability in the Central Andes and its relation to tropical Pacific and Atlantic forcing. *J. Geophys. Res.* **105**, 2000JD900134 (2000).
20. G. Seltzer, D. Rodbell, S. Burns, Isotopic evidence for late Quaternary climatic change in tropical South America. *Geology* **28**, 35-38 (2000).
21. F. W. Cruz *et al.*, Insolation-driven changes in atmospheric circulation over the past 116,000 years in subtropical Brazil. *Nature* **434**, 63-66 (2005). doi: 10.1038/nature03365.
22. B. Lemieux-Dudon *et al.*, Consistent dating for Antarctic and Greenland ice cores. *Quat. Sci. Rev.* **29**, 8-20 (2010). doi: 10.1016/j.quascirev.2009.11.010
23. C. Barbante *et al.*, One-to-one coupling of glacial climate variability in Greenland and Antarctica. *Nature* **444**, 195-198 (2006). doi: 10.1038/nature05301
24. J. Flückiger, $N_2O$ and $CH_4$ variations during the last glacial epoch: Insight into global processes. *Global Biogeochem. Cycles* **18**, GB1020 (2004). doi: 10.1029/2003gb002122
25. T. Blunier, E. J. Brook, Timing of millennial-scale climate change in Antarctica and Greenland during the last glacial period. *Science* **291**, 109-112 (2001).
26. J. Chappellaz *et al.*, Synchronous Changes in Atmospheric $CH_4$ and Greenland Climate between 40-kyr and 8-kyr BP. *Nature* **366**, 443-445 (1993).
27. A. Dallenbach *et al.*, Changes in the atmospheric $CH_4$ gradient between Greenland and Antarctica during the Last Glacial and the transition to the Holocene. *Geophys. Res. Lett.* **27**, 1005-1008 (2000).
28. M. Bock *et al.*, Hydrogen Isotopes Preclude Marine Hydrate $CH_4$ Emissions at the Onset of Dansgaard-Oeschger Events. *Science* **328**, 1686-1689 (2010). doi 10.1126/science.1187651
29. X. Wang *et al.*, Interhemispheric anti-phasing of rainfall during the last glacial period. *Quat. Sci. Rev.* **25**, 3391-3403 (2006). doi: 10.1016/j.quascirev.2006.02.009
30. X. F. Wang *et al.*, Wet periods in northeastern Brazil over the past 210 kyr linked to distant climate anomalies. *Nature* **432**, 740-743 (2004). doi: 10.1038/nature03067
31. J. A. Smith, D. T. Rodbell, Cross-cutting moraines reveal evidence for North Atlantic influence on glaciers in the tropical Andes. *J. Quat. Sci.* **25**, 243-248 (2010). doi: 10.1002/Jqs.1393
32. A. Jaeschke, C. Ruhlemann, H. Arz, G. Heil, G. Lohmann, Coupling of millennial-scale changes in sea surface temperature and precipitation off northeastern Brazil with high-latitude climate shifts during the last glacial period. *Paleoceanography* **22**, (2007). doi: 10.1029/2006pa001391
33. T. C. Jennerjahn *et al.*, Asynchronous terrestrial and marine signals of climate change during Heinrich events. *Science* **306**, 2236-2239 (2004). doi: 10.1126/science.1102490

34. J. C. H. Chiang, C. M. Bitz, Influence of high latitude ice cover on the marine Intertropical Convergence Zone. *Clim. Dyn.* **25**, 477-496 (2005). doi: 10.1007/S00382-005-0040-5
35. R. Zhang, T. L. Delworth, Simulated tropical response to a substantial weakening of the Atlantic thermohaline circulation. *J. Clim.* **18**, 1853-1860 (2005).
36. A. C. Clement, L. C. Peterson, Mechanisms of abrupt climate change of the last glacial period. *Rev. Geophys.* **46**, RG000204 (2008). doi: 10.1029/2006rg000204
37. G. H. Denton *et al.*, The Last Glacial Termination. *Science* **328**, 1652-1656 (2010). doi: 10.1126/science.1184119
38. R. F. Anderson *et al.*, Wind-Driven Upwelling in the Southern Ocean and the Deglacial Rise in Atmospheric CO(2). *Science* **323**, 1443-1448 (2009). doi: 10.1126/science.1167441
39. D. Roche, D. Paillard, E. Cortijo, Constraints on the duration and freshwater release of Heinrich event 4 through isotope modelling. *Nature* **432**, 379-382 (2004). doi: 10.1038/nature03059
40. A. J. Weaver, O. A. Saenko, P. U. Clark, J. X. Mitrovica, Meltwater pulse 1A from Antarctica as a trigger of the Bolling-Allerod warm interval. *Science* **299**, 1709-1713 (2003). doi: 10.1126/science.1081002
41. J. P. Sachs, S. J. Lehman, Subtropical North Atlantic temperatures 60,000 to 30,000 years ago. *Science* **286**, 756-759 (1999).
42. E. A. Boyle, Characteristics of the deep ocean carbon system during the past 150,000 years: CO2 distributions, deep water flow patterns, and abrupt climate change. *Proc. Natl. Acad. Sci. U.S.A.* **94**, 8300-8307 (1997).
43. L. C. Skinner, H. Elderfield, Rapid fluctuations in the deep North Atlantic heat budget during the last glacial period. *Paleoceanography* **22**, (2007). doi: 10.1029/2006pa001338
44. A. J. Broccoli, K. A. Dahl, R. J. Stouffer, Response of the ITCZ to Northern Hemisphere cooling. *Geophys. Res. Lett.* **33**, L01702 (2006). doi: 10.1029/2005gl024546
45. M. Stute *et al.*, Cooling of Tropical Brazil (5°C) during the Last Glacial Maximum. *Science* **269**, 379-383 (1995).
46. S. T. Kim, J. R. O'Neil, Equilibrium and nonequilibrium oxygen isotope effects in synthetic carbonates. *Geochim. Cosmochim. Acta* **61**, 3461-3475 (1997).
47. J. Imbrie *et al.*, in *The Orbital Theory of Pleistocene Climate: Support from a Revised Chronology of the Marine $\delta^{18}O$ Record*, A. Berger, Ed., Milankovitch and Climate, Part 1 (Hingham, MA, 1984).
48. R. Garreaud, M. Vuille, A. Clement, The climate of the Altiplano: observed current conditions and mechanisms of past changes. *Palaeogeogr. Palaeoclimatol. Palaeoecol.* **194**, 5-22 (2003). doi: 10.1016/s0031-0182(03)00269-4
49. R. D. Garreaud, M. Vuille, R. Compagnucci, J. Marengo, Present-day South American climate. *Palaeogeogr. Palaeoclimatol. Palaeoecol.* **281**, 180-195 (2009). doi: 10.1016/J.Palaeo.2007.10.032
50. J. Laskar *et al.*, A long-term numerical solution for the insolation quantities of the Earth. *Astronomy & Astrophysics* **428**, 261-285 (2004). doi: 10.1051/0004-6361:20041335
51. X. Wang *et al.*, Millennial-scale precipitation changes in southern Brazil over the past 90,000 years. *Geophys. Res. Lett.* **34**, (2007). doi: 10.1029/2007gl031149

**Acknowledgments:** This work is supported by NSF ATM-1003466 to SJB, NSF 0502535 and 1103403 to RLE and HC, and GSA Student Award 9308-10 to LCK. We thank Carlos Morales-Bermudez for his invaluable assistance in the field. Comments from two anonymous reviewers have significantly improved the manuscript. The data in this paper are tabulated in the supporting online material and are archived online at ftp://ftp.ncdc.noaa.gov/pub/data/paleo.

**Supporting Online Material**
www.sciencemag.org/cgi/content/full/science.1213397/DC1
Methods
Figs. S1 to S5
Table S1
References (*45–51*)

31 August 2011; accepted 4 January 2012
Published online 12 January 2012; 10.1126/science.1213397

**Fig. 1.** The $\delta^{18}O$ reconstruction of stalagmite P09-PH2 compared to high-latitude ice core $\delta^{18}O$ and methane concentrations. (**A**) GRIP and NGRIP methane (black) (*24*, *25*), and EDML methane (purple) (*23*) concentrations. (**B**) NGRIP ice core $\delta^{18}O$ (dark green, 7-pt running mean) (*22*). (**C**) Speleothem P09-PH2 $\delta^{18}O$ time series with U/Th dates with $2\sigma$ uncertainty bars (dark blue, 3-pt running mean). (**D**) EDML ice core $\delta^{18}O$ (red, 7-pt running mean) (*23*). The age models for Greenland and Antarctica $\delta^{18}O$ and NGRIP and EDML methane concentrations from (*22*). GRIP methane concentrations are shown on the GISP2 timescale from (*25*). The timescale of P09-PH2 is given on its own age model (see fig. S2). The Heinrich events are depicted by the vertical arrows and age estimations from (*4*, *7*). The numbers indicate Greenland interstadials and Antarctic AIM events.

**Fig. 2.** Detailed view of the oxygen isotope records from Pacupahuain Cave (blue) and Greenland (green) and Antarctic (red) ice cores during (**A**) Heinrich event 4 and D/O and AIM events 8 and (**B**) Heinrich event 5 and D/O and AIM events 12. Solid black line indicates the end of and dashed black lines indicate two possible onsets for Heinrich

events H4 and H5. Isotope records and corresponding age models are the same as in Fig. 1.

**Fig. 3.** Bermuda Rise SSTs (orange) shown to depth in core MD95-2036 (*41*). D/O events were identified on the basis of visual correlation to the Greenland isotope temperature record as in (*41*). Expanded view of results from our P09-PH2 record (orange) and subtropical Atlantic SSTs (blue) using our revised age model (*11*).

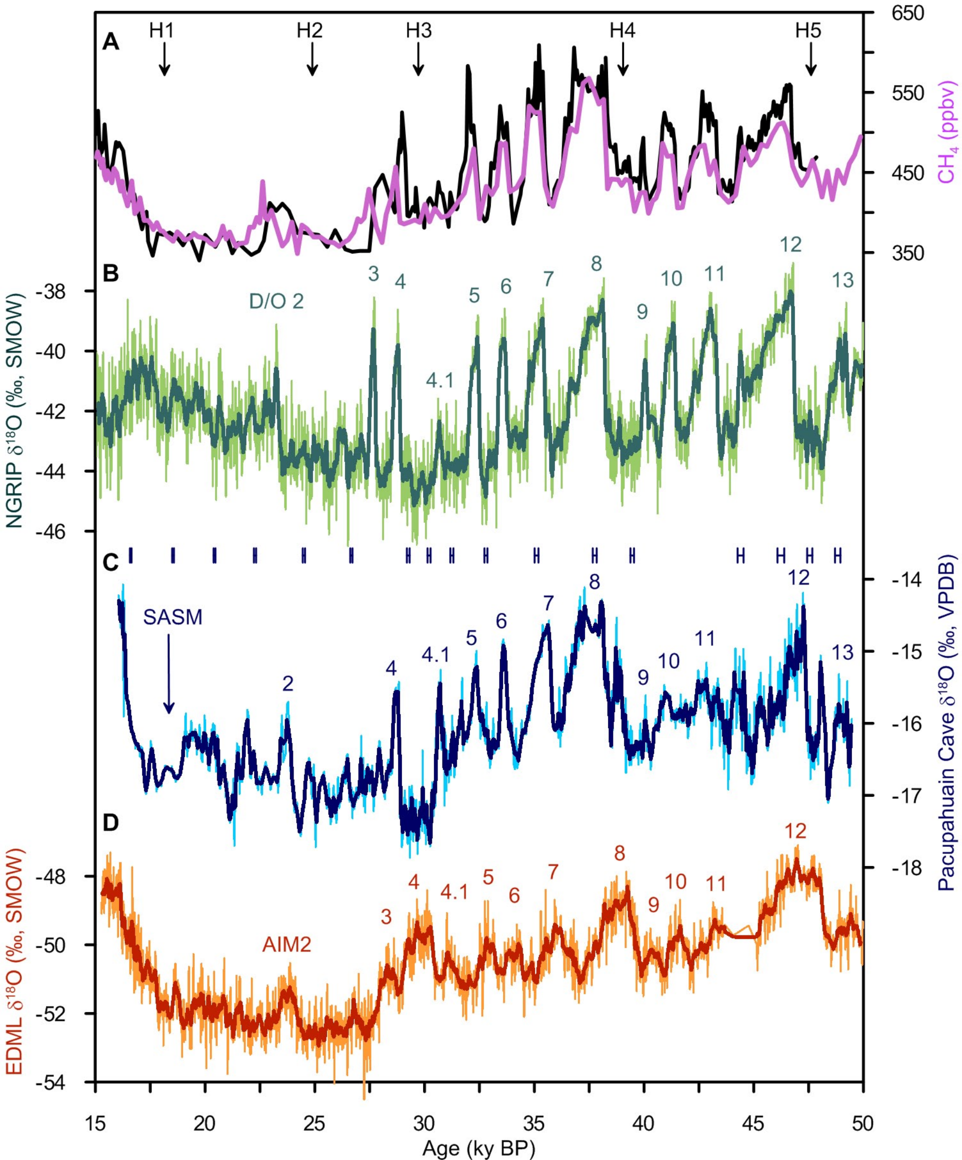
A
H1
H2
H3
H4
H5
$CH_4$ (ppbv)
650
550
450
350
B
NGRIP $\delta^{18}O$ (‰, SMOW)
D/O 2
3
4
4.1
5
6
7
8
9
10
11
12
13
-38
-40
-42
-44
-46
C
SASM
Pacupahuain Cave $\delta^{18}O$ (‰, VPDB)
-14
-15
-16
-17
-18
D
AIM2
EDML $\delta^{18}O$ (‰, SMOW)
-48
-50
-52
-54
15
20
25
30
35
40
45
50
Age (ky BP)

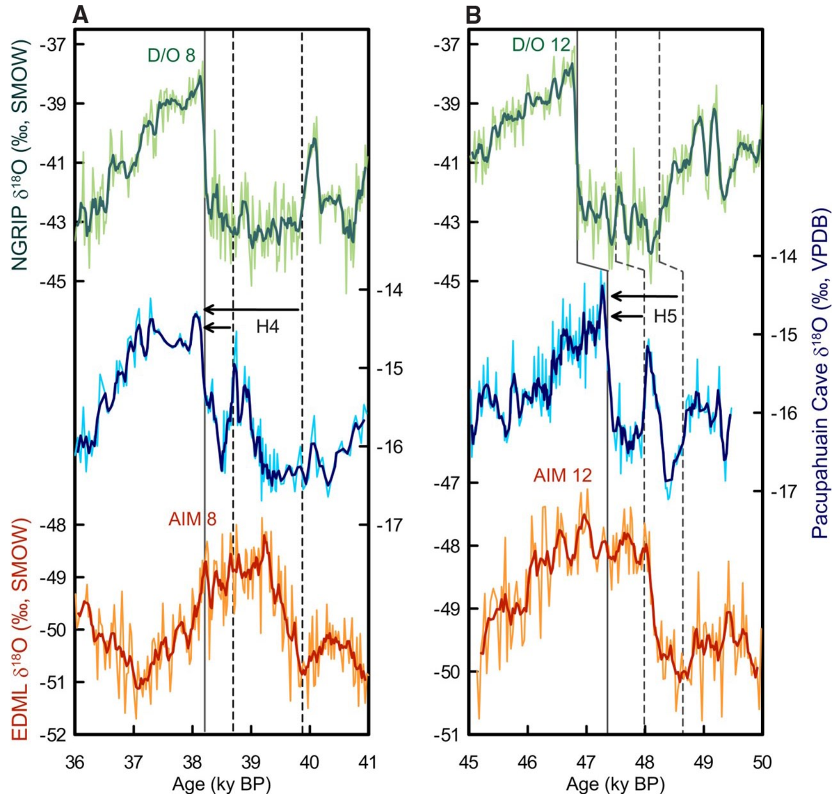

A
B
D/O 8
D/O 12
H4
H5
AIM 8
AIM 12
NGRIP δ18O (‰, SMOW)
EDML δ18O (‰, SMOW)
Pacupahuain Cave δ18O (‰, VPDB)
Age (ky BP)
Age (ky BP)

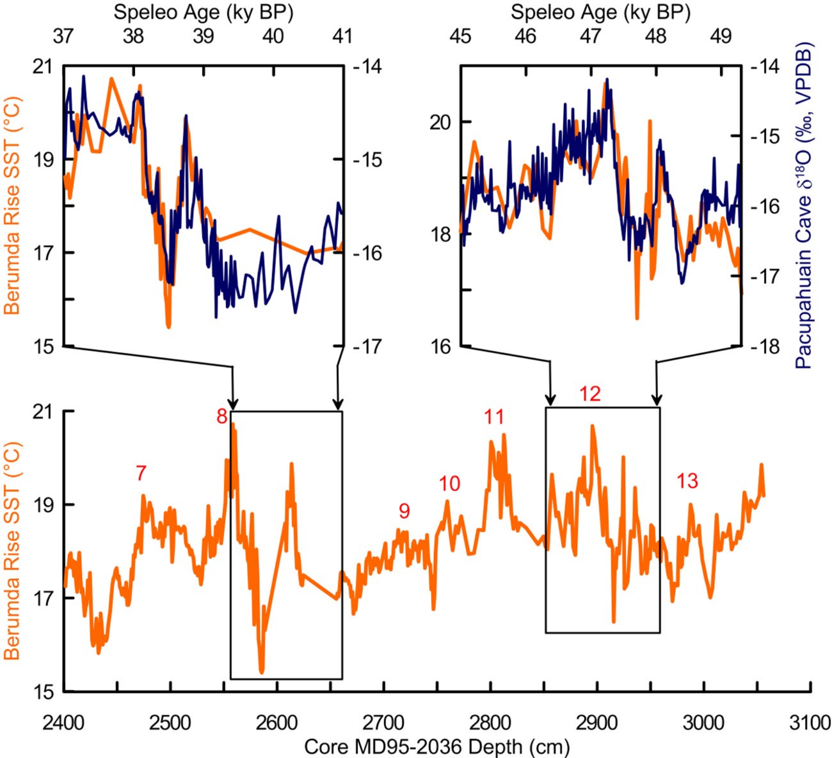

Speleo Age (ky BP)
37
38
39
40
41
Speleo Age (ky BP)
45
46
47
48
49
21
19
17
15
-14
-15
-16
-17
20
18
16
-14
-15
-16
-17
-18
Berumda Rise SST (°C)
Pacupahuain Cave δ18O (‰, VPDB)
21
19
17
15
Berumda Rise SST (°C)
7
8
9
10
11
12
13
2400
2500
2600
2700
2800
2900
3000
3100
Core MD95-2036 Depth (cm)